Emergent-angle-dependent charge-state distributions of 2-MeV ^{4}He transmitted through a thin carbon foil

H. Ogawa,* N. Sakamoto, N. Shiomi-Tsuda, and H. Tsuchida

Department of Physics, Nara Women's University, Nara 630, Japan

(Received 19 January 1999; revised manuscript received 21 September 1999; published 16 February 2000)

The emergent-angle-dependent charge-state fractions of 2-MeV ^{4}He transmitted in a carbon foil of 2.5 μg/cm^2 in thickness have been measured in the range from 0 to 8 mrad. The angular distribution due to multiple scattering has been also obtained for each outgoing charge state. Up to the angle of ~4 mrad, both the neutral and singly charged fractions increase with increasing the emergent angle. This trend is more remarkable in the neutral fraction. At the larger angles, these fractions reach saturated values. The observed behavior can be explained qualitatively by the impact parameter dependence of the charge-exchange probabilities. Although a Monte Carlo simulation can reproduce the obtained angle-dependent charge-state fractions, it gives a slightly narrower angular distribution due to multiple scattering for each outgoing charge state.

PACS number(s): 34.70.+e, 34.50.Fa

I. INTRODUCTION

In order to improve the understanding of atomic collisions of fast ions, the charge state of the projectile is one of the essential quantities to be investigated. As for a fast proton, the charge states in solids can be described by electron capture into and subsequent electron loss from bound states on the proton [1]. Furthermore, the equilibrium and nonequilibrium H^0 fractions emerging from carbon foils were found to be represented with the electron-loss and -capture cross sections derived by applying an additivity rule to the measurement with various carbon containing gas targets [1–4]. The measurements of the charge state fractions and their analysis based on the above-mentioned model have been performed also for He atoms or ions transmitted in thin carbon foils [5–7].

In contrast to the inclusive measurement of the charge state distributions of the foil-transmitted particles, the measurement of the angular dependence of the charge state fractions emerging from a solid can give us further details of the charge changing collisions. Although the incident particles experience a number of collisions with the atoms in the target medium, the charge state and the emergent angle of the transmitted particles reflect the individual collisions. Since the charge changing probabilities depend on the impact parameter, it is meaningful to examine how the impact parameter of the charge exchanges in a single collision comes out in the angle-dependent charge-state fractions of the foil-transmitted particles.

In the present work, the emergent angle-dependent charge-state fractions have been measured with 2-MeV ^{4}He particles transmitted in a thin carbon foil. The angular distributions due to multiple scattering are also presented for the individual outgoing charge states. The results are interpreted with the impact parameter dependence of the charge-exchange probabilities and are also compared with a Monte Carlo simulation.

---

*Author to whom correspondence should be addressed. FAX: +81 742 20 3380. Electronic address: ogawa@phys.nara-wu.ac.jp

II. EXPERIMENTAL PROCEDURE

The experiment was performed using the 1.7-MV Tandem Van de Graaff accelerator at Nara Women's University. The measurement was carried out for the incidence of both doubly and singly charged 2-MeV ^{4}He ions, separately. Figure 1 represents the experimental arrangement. The momentum analyzed beams were collimated with a couple of diaphragms S_1 and S_2. They were 0.3 mm in diameter and 224 cm apart from each other. The angular divergence of the incident beams was less than 0.14 mrad. In order to prevent the edge-scattered particles at the diaphragms S_1 and S_2 from hitting the target, a baffle S_3 of 1.0 mm in diameter was placed 10 cm behind the diaphragm S_2. The target carbon foil was placed 3 cm behind the baffle S_3.

The thickness of this foil was determined to be 2.5 $\pm$ 0.1 μg/cm^2 by the Rutherford backscattering method with 2-MeV α beams. By this Rutherford backscattering measurement, this foil was found to contain the contamination of oxygen atoms. However, the amount of this contamination was about 2 % carbon in units of atoms/cm^2, the effect of which on the measured charge-state fractions was negligibly small. Moreover, the amount of hydrogen atoms in the foil was examined by the elastic recoil detection analysis technique and was found to be about 10 % carbon in units of atoms/cm^2. The errors due to this contaminant are roughly estimated in Sec. III.

The emergent angle of the foil-transmitted particles was defined with a couple of slits S_V and S_H located about 70 cm
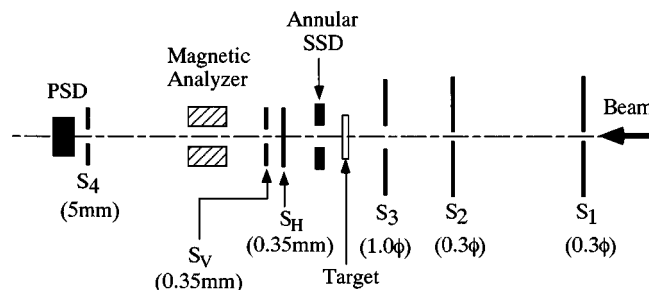

FIG. 1. Experimental arrangement.
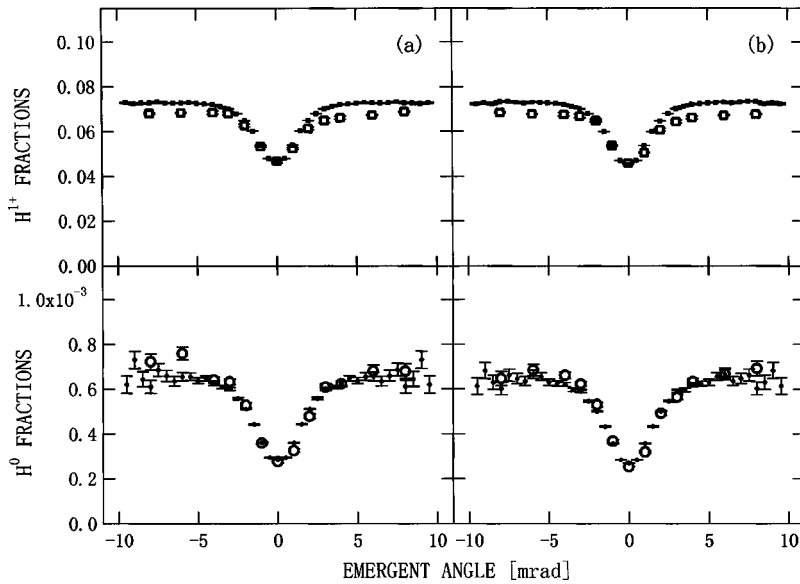
FIG. 2. The emergent-angle-dependent charge-state distributions of 2-MeV ^{4}He transmitted in a carbon foil of 2.5 μg/cm^2 for the incidence of He^{1+} (a) and He^{2+} (b). The circles and squares denote the fractions of the neutral and singly charged components, respectively. The open and solid symbols represent the results of the measurement and the computer simulation, respectively.

behind the target foil. Each of these slits was 0.35 mm in width. The slits S_H and S_V were movable horizontally and vertically, respectively, in the plane perpendicular to the incident beam axis. A magnetic analyzer separated horizontally the particles passing through these slits into three charge components, namely, the neutral, singly charged, and doubly charged ones. Finally, they were detected with a position-sensitive Si detector which was movable horizontally in accordance with the emergent angle. At the beginning of the measurement, the slits S_V and S_H were adjusted to the position of the incident beam by monitoring the beam spot at the detector position without the target foil and no magnetic field. In the measurement, the slit S_V was fixed at the position of the incident beams and the emergent angle was defined by the slit S_H. In order to diminish the effect of the residual magnetization in the vacuum chamber and the vacuum duct, and of the geomagnetism, the beam line between the target and the angle-defining slit was covered with a cylinder of μ metal. The measured angular range was from 0 to 8 mrad.

Throughout the measurement the counting rate of the detector was kept less than ~300 counts/s in order to avoid possible peak broadening of the charge-state distribution due to the pileup effect. For 2-MeV ^{4}He, the doubly charged fraction was more than 90%, but on the other hand, the neutral fraction was less than 0.1% in the equilibrium charge-state distribution. Therefore the simultaneous detection of the three charge components takes a lot of time to obtain good counting statistics for the neutral fraction. In order to improve this situation, another measurement was carried out with the intensified beam, where the detector position was adjusted at each emergent angle to detect only the single charged and neutral components.

The measurement was carried out at both the left and right side around the incident beam axis in the horizontal plane in order to examine that the zero emergent angle was accurately determined by the above-mentioned procedure. The amount of the incident beams was monitored by an annular-type silicon detector placed about 10 cm behind the target foil, and

the angular distribution due to multiple scattering was also determined for each outgoing charge state.

III. RESULTS AND DISCUSSION

Figures 2(a) and 2(b) represent the measured emergent angle dependence of the singly charged (squares) and the neutral (circles) fractions for the incidence of He^{1+} and He^{2+}, respectively. The positive and negative signs of the emergent angle correspond to the left and right side around the incident beam axis in the horizontal plane, respectively.

As mentioned in Sec. II, the carbon foil contained the hydrogen contaminant, the amount of which was about 10% carbon atoms in units of atoms/cm^2, that is to say, about 0.02 μg/cm^2 in thickness. According to the theory of the multiple scattering by Sigmund and Winterbon [8], the ratio of the scattering yield of 2-MeV He^{2+} ions at an angle θ to the zero emergent angle, $f(\theta)/f(0)$, transmitted a hydrogen target of 0.02 μg/cm^2 is two or three orders of magnitude smaller than that transmitted in a carbon foil of 2.5 μg/cm^2 at $\theta \geqslant 1$ mrad. Therefore the broadening of the angular distribution due to multiple scattering by this contaminant is very small. As for the electron loss of He^{1+} and the electron capture of He^{2+}, the total cross sections for hydrogen are more than one order of magnitude smaller than the corresponding ones for carbon [9,10]. With respect to the charge exchange between He^{1+} and He^0, the electron-loss and -capture cross sections for hydrogen are about 20% and 40% of those for carbon, respectively [9,10]. Considering these ratios and the amount of the hydrogen atoms, the error of the neutral fraction at each emergent angle due to the contaminant is evaluated to be about 4%. Those of the singly and doubly charged ones are estimated to be less than 1%. The associated errors of the fractions in Fig. 2 are just the statistical ones and do not contain the ambiguity due to the hydrogen contaminant.

As is clear from these figures, both the singly charged and neutral fractions at each emergent angle are almost independent of the incident charge state. This seems to suggest that the charge state of 2-MeV ^{4}He is equilibrated in the carbon

TABLE I. Electron loss and electron capture cross sections.

	Electron loss (units of πa_B^2)		Electron capture (units of πa_B^2)	
	σ_{01}	σ_{12}	σ_{10}	σ_{21}
Experiment	1.4×10^{0a}	6.4×10^{-1a}	9.5×10^{-4b}	3.5×10^{-2b}
Theory	1.1×10^{0c}	6.0×10^{-1c}	8.5×10^{-4d}	4.7×10^{-2d}

[a]Sataka, Yagishita, and Nakai, Ref. [12].
[b]Calculated from the electron-loss cross sections by Sataka, Yagishita, and Nakai [12] and the equilibrium charge-state fractions estimated from the present data.
[c]Calculated with the Bohr model [13,14].
[d]Calculated with the OBK approximation [16].

foil of 2.5 μg/cm^2. In order to ascertain this, the charge-state distributions were calculated as a function of the foil thickness using the three component model [11]. In this calculation, the charge changing cross sections employed are as follows. At first, the double electron capture of He^{2+} and the double electron loss of He^0 were neglected because they are expected to be sufficiently small compared to the competing single electron transfer cross sections [9,10,12]. For the electron-loss cross sections, the experimental data by Sataka, Yagishita, and Nakai [12] are available. When only the single electron transfer is considered, we can get the following relation

$$\frac{\sigma_{i+1,i}}{\sigma_{i,i+1}} = \frac{F_i}{F_{i+1}} \quad (i=0,1), \tag{1}$$

where σ_{ij} denotes the charge changing cross section from $i+$ to $j+$ and F_i is the equilibrium charge state fraction of $i+$. From the present results of the emergent-angle-dependent charge-state fractions and the angular distribution due to multiple scattering, F_1 and F_0 for 2-MeV ^{4}He in carbon are evaluated to be 5.2×10^{-2} and 3.5×10^{-4}, respectively. These values are the means of those for He^{1+} and He^{2+} incidence and agree with each other within the accuracy of 3% both for F_1 and F_0. With these values and $\sigma_{i,i+1}$'s by Sataka, Yagishita, and Nakai [12], we have determined the electron-capture cross sections. The numerical values of σ_{ij}'s used in the calculation are listed in Table I. Figures 3(a) and 3(b) show the calculated charge state distributions for He^{1+} and He^{2+} incidence, respectively. The vertical lines in the figures denote the foil thickness employed in this measurement. The charge-state equilibrium is realized almost completely at this thickness.

As is clear from Figs. 2(a) and 2(b), not only the singly charged but also the neutral fractions increase with increasing the emergent angle from 0 to ~4 mrad. This trend is more remarkable in the neutral fraction. At the larger angle, these fractions appear to reach saturated values. The observed angle dependence is expected to reflect the impact parameter dependence of the electron-loss and electron-capture probabilities of 2-MeV He colliding with a carbon atom.

Figures 4(a) and 4(b) represent the angular distribution due to multiple scattering of each outgoing charge state for
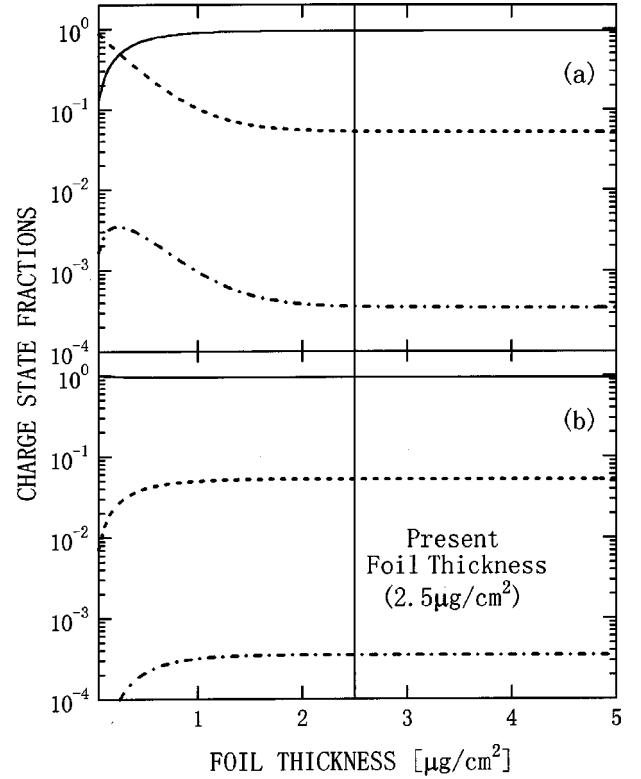

FIG. 3. The calculated charge-state distribution of 2-MeV ^{4}He as a function of the carbon foil thickness for the incidence of He^{1+} (a) and He^{2+} (b). The solid, dashed, and dash-dotted curves represent the fraction of doubly charged, singly charged, and neutral components, respectively. The vertical lines denote the thickness of the carbon foil employed in the present measurement.

He^{1+} and He^{2+} incidence, respectively. The distributions are normalized by the yields at 0 mrad. The measured distribution for He^{1+} becomes slightly broader compared with that for He^{2+} and this broadening is further enhanced for He^0. This behavior reflects exactly the same nature as the emergent angle dependence of the charge-state fractions.

In order to look into further details, we have calculated the impact parameter dependence of the electron-loss and -capture probabilities. The electron-loss probabilities of He^{1+} and He^0 were estimated with the classical model by Bohr [13,14], where the contribution from the target nucleus and its bound electrons are taken into account independently. Figure 5 represents the schematics of the coordinate system to calculate the electron-loss probabilities. The coordinates are those projected on the plane perpendicular to the incident beam. At first, we consider the collision of a bound electron to the projectile nucleus with a screened target nucleus, whose screened potential is written by

$$V(r_T) = \frac{Z_T e^2}{r_T} \exp\left(-\frac{r_T}{Z_T^{-1/3} a_B}\right), \tag{2}$$

where Z_T and a_B denote the target atomic number and the Bohr radius. According to the theory by Bohr [13], when the electron bound to the projectile is regarded as a free electron, the relation of the impact parameter between the projectile
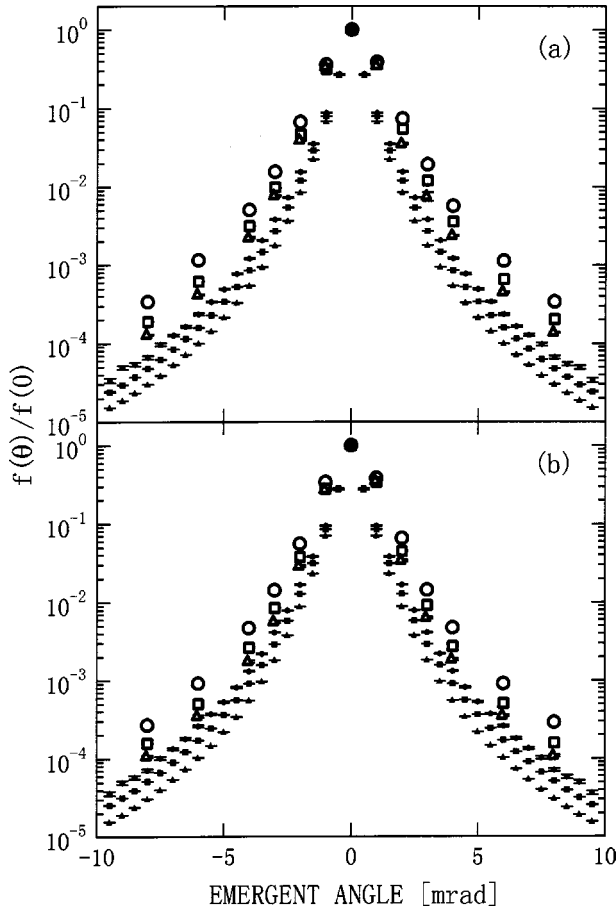
FIG. 4. The angular distributions due to multiple scattering of 2-MeV ^{4}He transmitted in a carbon foil of 2.5 μg/cm^2 for the incidence of He^{1+} (a) and He^{2+} (b). The circles, squares, and triangles denote the outgoing fractions of the neutral, singly, and doubly charged components, respectively. The open and solid symbols represent the results of the measurement and the computer simulation, respectively.

bound electron and the screened target nucleus, b_{e-s}, and the scattering angle of the electron, θ_{CM}, in the center of mass frame is given by

$$\theta_{CM} = \frac{\pi}{2e_N} \frac{2Z_T e^2}{mV^2} \frac{a_B Z_T^{-1/3}}{b_{e-s}^2}, \tag{3}$$
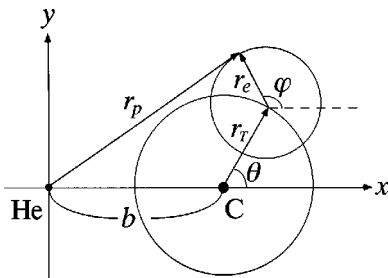

FIG. 5. The schematics of the coordinate system to calculate the electron-loss probability. The coordinates are those projected on the plane perpendicular to the incident beam.

where V and m are the projectile velocity and the rest mass of an electron, respectively. e_N denotes the base of natural logarithm. When the transferred energy to the electron exceeds its binding energy, the electron is released from the projectile nucleus. The maximum impact parameter between the electron and the target nucleus, b_n, for the projectile ionization is expressed by

$$b_n \sim a_B Z_T^{1/3} v_B (V v_I)^{-1/2}, \tag{4}$$

where v_B and v_I are the Bohr velocity and the orbital velocity of the electron in the ground state of He. For He^0, v_I was obtained from the Dirac-Fock orbital energy by Desclaux [15]. At a given impact parameter, b, between the projectile and target nuclei, the electron-loss probability by the target nucleus $P_l^n(b)$ is given by

$$P_l^n(b) = \int_0^{b_n} r_T dr_T \int_0^{2\pi} d\theta \, \rho_P(r_P), \tag{5}$$

where $\rho_P(r)$ is the probability density of the electron of He projected on the plane perpendicular to the incident axis and was calculated from the ground-state hydrogenic wave function with the eigenvalue of the Dirac-Fock orbital energy [15].

As for the contribution from the target electrons, the binary encounter of electrons is considered. The criterion for the projectile ionization is the same as considered in the collision with the target nucleus. The upper limit of the impact parameter, b_e, between the electrons is given by

$$b_e = 2a_B(v_B/V)^2 [(V/v_I)^2 - 1]^{1/2}. \tag{6}$$

The electron loss probability by the target electrons $P_l^e(b)$ is given by

$$P_l^e(b) = \int_0^\infty r_T dr_T \int_0^{2\pi} d\theta \, \rho_T(r_T) \int_0^{b_e} r_e dr_e \int_0^{2\pi} d\varphi \, \rho_P(r_P), \tag{7}$$

where $\rho_T(r)$ is the total probability density of the 1s, 2s, and 2p electrons of a carbon atom projected on the plane perpendicular to the incident axis and was also calculated from the hydrogenic wave function with the eigenvalue of the Dirac-Fock orbital energy [15]. Finally, the total electron-loss probability is given by the sum of $P_l^n(b)$ and $P_l^e(b)$.

The electron-capture probabilities of He^{2+} and He^{1+} ions were calculated with the well-known Oppenheimer-Brinkman-Kramers (OBK) approximation [16]. The electron capture from 1s, 2s, and 2p subshells of a carbon atom to the ground state of He was considered. The hydrogenic wave functions with the eigenvalue of the Dirac-Fock orbital energy [15] was also employed for the initial and final states of the electron to be captured. Figure 6 represents the impact parameter dependence of the calculated electron-loss and -capture probabilities. The total cross sections are also listed in Table I.

From the calculated impact parameter dependence of the charge exchange, the following explanation can be made
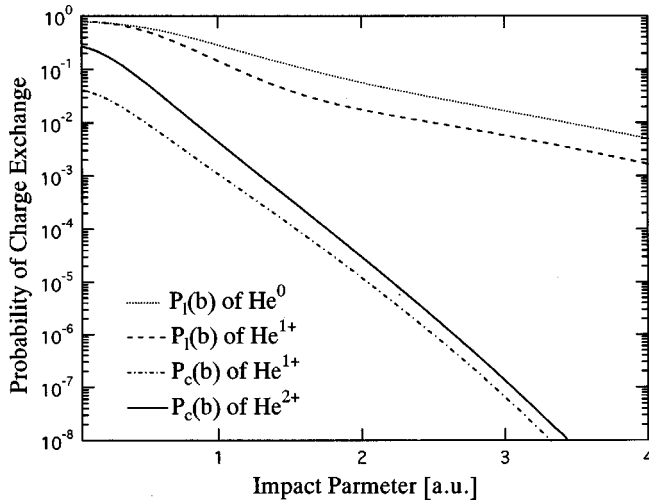
FIG. 6. The impact parameter dependence of charge-exchange probabilities in the collision of a 2-MeV ^{4}He particle with a carbon atom. The dashed and dotted curves represent the single electron-loss probabilities of He^{1+} and H^{0+}, respectively, calculated with the classical model by Bohr [13,14]. The solid and dash-dotted curves denote the single electron-capture probabilities of He^{2+} and He^{1+}, respectively, calculated with the OBK approximation [16].

with respect to the qualitative nature of the observed angle dependence of the charge-state fractions. Although the emergent angle is determined by the accumulation of successive collisions, the particles emerging at the small angle are subject, on the average, to the collisions of large impact parameter and vice versa. As seen in Fig. 6, at the large impact parameter region of $b \gtrsim 1.5 a_B$ the electron-capture probability increases more rapidly with decreasing the impact parameter compared with the electron-loss probability. This fact will cause the increase of He^{1+} and He^0 fractions up to ~ 4 mrad. On the other hand, in the small impact parameter region of $b \lesssim 0.05 a_B$, the charge-exchange probabilities approach gradually the maximum values at the zero impact parameter. In this connection, a deflection angle of 4 mrad corresponds to a single collision of $b \simeq 0.04 a_B$ for 2-MeV He^{2+} scattered from a carbon atom. Furthermore, in this region a small decrease of the impact parameter gives rise to a large increase of the scattering angle. Therefore it is reasonable that the He^0 and He^{1+} fractions are expected to saturate at the larger emergent angles. Since the He^0 component is mainly produced by the single electron capture of He^{1+}, the angle dependence of He^0 is strongly affected by that of He^{1+} in addition to the impact parameter dependence of the charge-exchange probability. Therefore the He^0 fraction exhibits more prominent emergent angle dependence.

Finally, the emergent-angle-dependent charge-state distributions were examined by a Monte Carlo simulation with the following procedure. The relation between the impact parameter and the scattering angle was determined with the Molière potential

$$V(r) = \frac{Z_P Z_T e^2}{r} \sum_{i=1}^{3} \alpha_i \exp\left(-\frac{\beta_i r}{a_{TF}}\right), \quad (8)$$

where Z_P and Z_T denote the atomic numbers of projectile and target atoms, respectively. The parameters α_i and β_i are given by $(\alpha_1, \alpha_2, \alpha_3) = (0.35, 0.55, 0.10)$ and $(\beta_1, \beta_2, \beta_3) = (0.3, 1.2, 6.0)$. For the interaction between the neutral atoms, the Thomas-Fermi screening radius, a_{TF}, is given by

$$a_{TF} = \frac{0.88534 a_B}{(Z_P^{1/2} + Z_T^{1/2})^{2/3}}. \quad (9)$$

For a projectile with no bound electron, the denominator of the right-hand side of Eq. (3) is replaced by $Z_T^{1/3}$. In the present calculation, Z_P was taken to be unity for He^{1+}. For a charge changing collision, the scattering angle at that collision was regarded as the mean of those for the elastic collisions with the initial and final charge states.

As for the charge-exchange probabilities, we have used the impact parameter dependence given in Fig. 6. Here, the absolute values of the probabilities used in the simulation were normalized so that the theoretical total cross sections agree with those used in the calculation of the foil thickness dependence of the charge-state distributions.

The procedure of the computer simulation is as follows. Target atoms were assumed to be spheres of radius R and to be distributed randomly. If a projectile traverses these spheres, it is scattered by the target atoms and at the same time its charge state may be changed. At first, the depth where the first collision occurred was determined by a pseudorandom number produced in the computer and then the impact parameter on this collision and the direction of the scattering were also determined with two other pseudorandom numbers. Here, the polar and azimuthal angles of the scattering with respect to the incident direction were recorded. With the impact-parameter-dependent charge-exchange probabilities described above, the charge state of the projectile after the collision was also determined. Next, the path length to the subsequent collision, the resultant scattering angle and the charge state were determined in the same manner and the results were recorded. These procedures were repeated until the projectile reached the outside of the target foil and then the final charge state was registered. The total deflection angle was calculated from the polar and azimuthal angles in the individual collisions using the approximation described in Ref. [17].

Here, the target radius R is expected to be a key parameter of the simulation because it corresponds to the upper limit of the impact parameter within which the deflection and the charge exchange of the projectile should be considered. It also determined the mean free path of the projectile in the foil. In the present simulation, R was taken to be $4a_B$, where the electron-loss probability falls below 1%. In this connection, it was ascertained that the preliminary simulation with $R = 2a_B$ presented about the same result as that with $R = 4a_B$. In order to obtain tolerable statistics for the He^0 yields at the large emergent angle, 10^9 particles were simulated both for He^{1+} and He^{2+} incidence.

The solid symbols in Figs. 2 and 4 represent the results of the simulation. The associated errors are statistical ones. The simulation can reproduce well the measured emergent angle dependence both for He^{1+} and He^0 fractions. As for the an-

gular distribution due to multiple scattering, however, the simulation gives a slightly narrower distribution than the measured one for each charge state. The partial disagreement with the experimental results might be originating from the imperfection of the charge exchange probabilities or the relation between the impact parameter and the scattering angle employed in the simulation.

IV. SUMMARY

The emergent-angle-dependent charge-state distribution of 2-MeV ^{4}He particles transmitted a carbon foil of 2.5 μg/cm^2 were measured both for He^{1+} and He^{2+} incidence. The angular distribution due to multiple scattering for each outgoing charge state was also obtained. The measured fraction at each angle is almost independent of the incident charge state. This is attributed to the fact that the charge state of the projectiles is well equilibrated in the foil. Not only the neutral but also singly charged fractions increased with increasing the emergence angle up to $\sim$4 mrad. This angle

dependence is more remarkable in the neutral fraction. At the larger emergent angle these fractions reach the saturated values. This behavior can be qualitatively explained by the impact parameter dependence of the electron-loss and -capture probabilities calculated with the Bohr model and the OBK approximation, respectively. Although a Monte Carlo simulation can reproduce well the angle-dependent charge-state fractions, it gives slightly narrower distribution than the measured one for each charge state. This kind of experiment is very important to investigate the impact parameter dependence of charge changing probabilities.

---

[1] M. C. Cross, Phys. Rev. B **2**, 602 (1977).

[2] A. Chateau-Thierry and A. Gladieux, in *Atomic Collision in Solids*, edited by S. Datz, B. R. Appleton, and C. D. Moak (Plenum, New York, 1975), p. 307.

[3] K. H. Berkner, I. Bornstein, R. V. Pyle, and W. Stearns, Phys. Rev. A **6**, 278 (1972).

[4] L. H. Toburen, M. Y. Nakai, and R. A. Langley, Phys. Rev. **171**, 114 (1968).

[5] N. Cue, N. V. de Castro Faria, M. J. Gaillard, J. C. Poizat, and J. Remillieux, Nucl. Instrum. Methods **170**, 67 (1980).

[6] A. Clouvas, M. J. Gaillard, A. G. de Pinho, J. C. Poizat, and J. Remillieux, Nucl. Instrum. Methods Phys. Res. B **2**, 273 (1984).

[7] H. Ogawa, N. Sakamoto, I. Katayama, I. Sugai, Y. Haruyama, M. Saito, K. Yoshida, Y. Susuki, and K. Kimura, Nucl. Instrum. Methods Phys. Res. B **135**, 87 (1998).

[8] P. Sigmund and K. B. Winterbon, Nucl. Instrum. Methods **119**, 541 (1974).

[9] P. Hvelplund and E. H. Pedersen, Phys. Rev. A **9**, 2434 (1974).

[10] L. I. Pivovar, T. M. Novikov, and V. M. Tavaev, Zh. Eksp. Tear. Fiz. **41**, 26 (1961) [Sov. Phys. JETP **14**, 20 (1962)]; **42**, 1490 (1962); [**15**, 1035 (1962)].

[11] S. K. Allison, Rev. Mod. Phys. **30**, 1137 (1973).

[12] M. Sataka, A. Yagishita, and Y. Nakai, J. Phys. B **23**, 1225 (1990).

[13] N. Bohr, K. Dan. Vidensk. Selsk. Mat. Fys. Medd. **18**, 8 (1948).

[14] Y. Fujii, K. Sueoka, K. Kimura, and M. Mannami, J. Phys. Soc. Jpn. **58**, 2758 (1989).

[15] J. P. Desclaux, At. Data Nucl. Data Tables **12**, 311 (1973).

[16] M. R. C. Mcdowell and J. P. Coleman, *Introduction to the Theory of Ion-Atom Collisions* (North-Holland, Amsterdam, 1970).

[17] N. Sakamoto, N. Shiomi, and R. Ishiwari, Phys. Rev. A **27**, 810 (1983).